An Improved Social Force Model Considering View Angle for Microscopic Pedestrian Simulation

Wenyao An
School of Transportation & Logistics
Southwest Jiaotong University
Chengdu, China
Anwenyao@my.swjtu.edu.cn

Shuiwang Chen
School of Transportation & Logistics
Southwest Jiaotong University
Chengdu, China
Chen.s.w@my.swjtu.edu.cn

Yan Li
School of Transportation & Logistics
Southwest Jiaotong University
Chengdu, China
LiYan@my.swjtu.edu.cn

Kai Peng
School of Transportation & Logistics
Southwest Jiaotong University
Chengdu, China
pengkai@my.swjtu.edu.cn

Lu Hu*
School of Transportation & Logistics
Southwest Jiaotong University
Chengdu, China
hulu@swjtu.edu.cn

2021 6th International Conference on Transportation Information and Safety (ICTIS) | 978-1-6654-9713-8/21/$31.00 ©2021 IEEE | DOI: 10.1109/ICTIS54573.2021.9798511

***Abstract*—This paper proposes an Improved Social Force Model (ISFM) considering the pedestrian and obstacle neighborhoods to simulate the micro-behavior of pedestrians in different scenes. Specially, the proposed model also considers different view angle sensitivities of one pedestrian to other obstacles and pedestrians. A simulation algorithm is proposed for the ISFM, which reduces the algorithm's complexity from polynomial complexity to linear complexity of pedestrian amount. Finally, a complex scene of metro passengers alighting and boarding the train is implemented to demonstrate the performance and efficiency of the ISFM. The result shows that the proposed algorithm improves the simulation efficiency while maintaining the accuracy of the original model.**

Keywords—pedestrian simulation, social force model, pedestrian view angle, simulation algorithm

I. INTRODUCTION

With the development of society and economy, the scale of cities is constantly expanding, and people's travel is more and more frequent. Urban rail transit has become the primary mode of transportation in megacities and big cities. How to guarantee the order and safety of the pedestrian flow is the problem that the traffic organizers pay attention to. At the same time, to meet the needs of safe, comfortable, and efficient pedestrian travel, planners and engineers need to carry out reasonable pedestrian traffic planning. Pedestrian micro-simulation is a tool to analyze the rationality of planning schemes. The development of computer performance makes large-scale pedestrian simulation possible. In computer simulation, researchers have proposed a variety of simulation models.

According to the different modeling perspectives, the pedestrian simulation models can be classified into the macro-simulation model, meso-simulation model, and micro-simulation model. Firstly, the macro model mainly regards the pedestrian as a fluid flow and focuses on the relationship between pedestrian speed, density, and flow. Macro-model can be used to study the pedestrian flow in different facility environments [1]. Through the relationship among the three parameters of speed, flow, and pedestrian density, the planning situation or service level of traffic configurations can be evaluated, which is of great significance to planning the layout of traffic configurations. Many simulation experiments are designed to study the regularity and characteristics of multidirectional pedestrian flow and the pedestrian flow at the bottleneck [2]. Secondly, the meso-model is between the macro model and the micro model. This model has a good application value in analyzing regional pedestrian simulation, such as evacuation path management [3]. Thirdly, micro-models mainly describe the details of pedestrian movement and can be used to study more complex pedestrian traffic flow problems. The micro-simulation model can be classified into the discrete model and continuous model.

In past decades, there are extensive researches on the pedestrian micro-simulation model. In order to describe the randomness and space occupancy of pedestrian walking, some researchers proposed a cellular automata model, which was further applied as a lattice gas model [4]. Some researchers have developed a pedestrian flow simulation model considering optimal control and differential game [2]. Regarding the force model, some researchers put forward a magnetic field force model, which believes that the pedestrian and the obstacle areas the same pole and the Exit as the opposite pole [5]. In line with the principle that opposites attract and same repel each other, pedestrian evacuation simulation is completed.

Unlike previous studies, a Social Force Model (SFM) based on the forces between people is proposed [6], and the research suggests that the movement of pedestrians could be regarded as composed of the driving force of pedestrians themselves, the interaction force between pedestrians, and the force between pedestrians and obstacles [7]. The microsimulation model was initially designed to simulate the walking behavior of pedestrians, that is, to integrate the psychological characteristics of pedestrians so that pedestrians could complete their movement under the joint action of various social forces. Due to the diversity of the traffic environment and the randomness of pedestrian walking behavior, the SFM was improved in many perspectives and applied to several traffic fields. A study has recalibrated the parameters and distributions of the SFM using the nonlinear regression method based on the data from the Massachusetts Institute of Technology student pedestrian flow experiment [8]. Some studies have focused on the application of SFM in different scenarios, such as ship disasters [9], multi-exit rooms [10], metros [11], passways, bottlenecks [12], evacuations [13], etc. The SFM is improved by taking advantage of the features of pedestrians walking with targets (evacuation, store, seat, and meeting place) [14].

978-1-6654-9713-8/21/$31.00 ©2021 IEEE

Some studies have improved the SFM itself. The tangential characteristic time of motion direction change was calibrated by practical experiment [15]. Setting the generalized walking cost to determine the dynamic navigation in the process of pedestrian evacuation [16]. Others have modified the friction coefficient to make the model fit the empirical data and distribution [17].

The SFM has been continuously improved and developed by different research. However, previous studies on the SFM mainly focus on modifying and optimizing model parameters, acting force and changing the acting force according to the specific environment. Few models consider the view angle sensitivity and algorithm for SFM. Therefore, there is a knowledge gap in considering the view angle sensitivity and the detail algorithm optimization for the SFM from the computational aspect. In this paper, the concepts of pedestrian and obstacle neighborhoods are proposed to improve the SFM considering view angle, and a detailed algorithm for our proposed model is also proposed.

The rest of this paper is organized as follows. Section II gives the original SFM and improves it by introducing pedestrian and obstacle neighborhoods. Then, section III develops an algorithm for the proposed ISFM. In section IV, a series of simulation experiments are implemented to demonstrate the efficiency and performance of the proposed model and algorithm. Finally, some conclusions and further studies are presented in section V.

II. IMPROVED SOCIAL FORCE MODEL

In this section, we first introduce the original SFM and analyze some details about this model. Then, according to the actual situation, the original SFM is improved in three aspects. The improved model can more truthfully simulate the movement behavior of individuals and groups under the interaction of multiple pedestrians.

A. Original SFM

The SFM was first proposed and improved by Helbing and Molnar. Helbing holds that people's movement trend and behavior can be abstracted as the movement of a mass particle, which is subjected to different forces at every moment. The interaction of these forces determines the motion and acceleration direction of the particle at that moment. Helbing divided the forces that people are subjected to into four categories: the self-driving force that drives pedestrians to reach the destination, the mutual repulsive force between different pedestrians, the repulsive force between pedestrians and obstacles, and the attraction between pedestrians. In this paper, the first three typical forces are selected for the study. At time t, the force exerted on pedestrian i can be formulated as the Eq.(1):

$$m_i \frac{d\vec{v}_i}{dt} = \vec{F}_i = \vec{F}_i^d + \vec{F}_i^p + \vec{F}_i^o \tag{1}$$

where m_i denotes the bodyweight of pedestrian i (i is the index of pedestrians, and pedestrian i is simply denoting as i in below), $\vec{v}_i$ denotes the speed of i, $\vec{F}_i$ denotes the resultant force of i, $\vec{F}_i^p$ denotes the driving force of i moving towards the destination, $\vec{F}_i^p$ denotes the repulsive force of other pedestrians on i, and $\vec{F}_i^o$ denotes the repulsive force on i from the obstacle.

1) Self-driving Force

The expression of pedestrians' self-driving force shows the tendency of pedestrians' expectation to move forward to their destination, as shown in Eq. (2) :

$$\vec{F}_i^{(d,t)} = m_i \frac{v_i^e \vec{e}_i^t - \vec{v}_i^t}{\tau_i} \tag{2}$$

where $\vec{F}_i^{(d,t)}$ is the self-driving force of i at time t, v_i^e denotes the expected speed of i (maximum speed), $\vec{e}_i^t$ denotes the anticipated movement direction of i, $\vec{v}_i^t$ denotes the speed of i at time t, and τ_i denotes the reaction time of i.

2) Interaction Force between Pedestrians

Pedestrians expect not to get too close to others when they move, which is shown in the model that other pedestrians will produce a repulsive force on i. This repulsive force keeps pedestrians at a reasonable distance from each other. The repulsive force of i by pedestrian j (j is the index of pedestrians) at time t is denoted by f_{ij}^t, it can be formulated as Eq.(4):

$$\vec{F}_i^{(p,t)} = \sum_{j(i\neq j)} f_{ij}^t \tag{3}$$

$$f_{ij}^t = \vec{n}_{ij}^t \left\{ A_i \exp\left(\frac{r_{ij} - d_{ij}^t}{B_i} \right) + Kg\left(r_{ij} - d_{ij}^t \right) \right\} + kg\left(r_{ij} - d_{ij}^t \right) \Delta v_{ji}^t \vec{t}_{ij} \tag{4}$$

where $\vec{n}_{ij}^t$ denotes the unit vector of j pointing to i; A_i and B_i are constants of i; $r_{ij} = r_i + r_j$, denotes the sum of the radius of i and j; d_{ij}^t is the distance between i and j at time t; $\Delta v_{ji}^t = \left(\vec{v}_j - \vec{v}_i \right) \cdot \vec{t}_{ij}$ denotes the velocity difference between i and j in the tangent direction; $\vec{t}_{ij}$ denotes the tangent direction of i and j. K is the elasticity coefficient of the human body, and k is the sliding friction coefficient of passenger, both of which are constant. $g(x)$ is a piecewise function, for $r_{ij} \geq d_{ij}$ or $r_i \geq d_{io}$, $g(x) = 0$; otherwise, $g(x) = x$.

$$g(x) = \begin{cases} 0, & r_{ij} < d_{ij} \vee r_i < d_{io} \\ x, & r_{ij} \geq d_{ij} \vee r_i \geq d_{io} \end{cases} \tag{5}$$

3) Resistance Force from Obstacles

When the pedestrian approaching the obstacle, he will be subjected to the repulsive force in the perpendicular and the tangent direction of the obstacle. $\vec{n}_{io}^t$ denotes the unit vector perpendicular to the direction of the obstacle and $\vec{t}_{io}$ denotes the unit vector tangent to the obstacle surface. The force of obstacle on i can be formulated as the following Eq.(6):

$$f_{io}^t = \vec{n}_{io}^t \left\{ A_i \exp\left(\frac{r_i - d_{io}^t}{B_i} \right) + Kg\left(r_i - d_{io}^t \right) \right\} - kg\left(r_i - d_{io}^t \right) \left(\vec{v}_i \cdot \vec{t}_{io} \right) \vec{t}_{io} \tag{6}$$

978-1-6654-9713-8/21/$31.00 ©2021 IEEE

B. Improved Social Force Model

In the previous section, the original SFM was analyzed. Although the original SFM can show the movement behavior of pedestrians in rich detail, there are still some inconsistent situations in the calculation process of each force. The original SFM is improved from three aspects to make the model a more refined description of pedestrian movement.

1) The neighborhood

In reality, the initial position of pedestrians is randomly distributed, and the position between different pedestrians changes with the environmental setting change. During time $\Delta\tau$, the speed and position of i changes are shown as follows:

$$\vec{v}_i^{t+\Delta\tau} = \vec{v}_i^t + \int_t^{t+\Delta\tau} \vec{a}_i^t dt \tag{7}$$

$$\vec{\gamma}_i^{t+\Delta\tau} = \vec{\gamma}_i^t + \int_t^{t+\Delta t} \vec{v}_i^t dt \tag{8}$$

In the original SFM, the repulsive pedestrian force of i is the sum of all other pedestrians' repulsive forces in the system. It is easy to design a program but does not match the actual pedestrian movement scene. For example, in the process of actual pedestrian movement, the moving direction of i is only affected by the movement state and destination of the pedestrians around him/her, and has no relationship with the movement state of other pedestrians far away from i in the whole system. We use pedestrian neighborhood to describe it in this paper (i.e., pedestrians only pay attention to the changes of things around them in the movement process). Pedestrians have different sensitivities to other pedestrians and obstacles. People are more sensitive to pedestrians because they are moving, while obstacles remain stationary in most scenes. Therefore, this paper introduces neighborhood pedestrian set NP^t and neighborhood obstacle set NO^t, and makes the following changes based on the original SFM:

$$NP_i^t = \left\{ j \left| \left| r_j^{(t,x)} - r_i^{(t,x)} \right| \le 2 \ \wedge \ \left| r_j^{(t,y)} - r_i^{(t,y)} \right| \le 2 \right. \right\} \quad \forall i, j \in P, t \in T \tag{9}$$

$$NO_i^t = \left\{ o \left| \left| r_o^{(t,x)} - r_i^{(t,x)} \right| \le 0.5 \ \wedge \ \left| r_o^{(t,y)} - r_i^{(t,y)} \right| \le 0.5 \right. \right\} \quad \forall i \in P, o \in O, t \in T \tag{10}$$

$\vec{r}_i^t = \left(r_i^{(t,x)}, r_i^{(t,y)} \right)$, where $\vec{r}_i^t$ denotes the location of i at time t; $r_i^{(t,x)}$ and $r_i^{(t,y)}$ are the components of $\vec{r}_i^t$ on the x and y axes, respectively. $\vec{r}_o = \left(r_o^x, r_o^y \right)$, denotes the location of obstacle o; r_o^x and r_o^y are the components of $\vec{r}_o$ on the x and y axes, respectively. Where P is the set of all pedestrians, and O is the set of all obstacles. Fig.1 shows the neighborhood pedestrian set and neighborhood obstacle set.

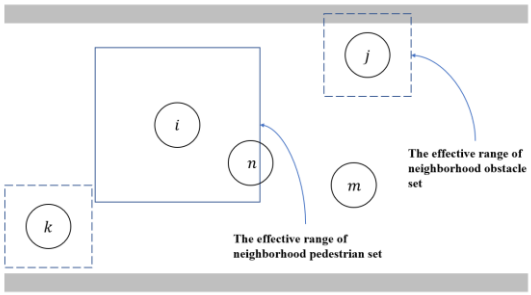

Fig. 1. neighborhood pedestrian set and neighborhood obstacle set

As shown in Fig.1(In this paragraph, i, j, n, m, k is the index of pedestrian), the neighborhood range of pedestrian i for other pedestrians is within the solid line square box, so the neighborhood pedestrian set of i at this moment only includes n. This paper believes that j, m and k, which are not in the neighborhood of i do not influence the movement track of i at this moment. The dashed line square box denotes the pedestrian's neighborhood of obstacles at this moment. For example, the movement path of j is affected by obstacles, while that of k is not.

The neighborhood pedestrian set and neighborhood obstacle set of i at time t can be calculated by Eq.(9) and(10). The calculation range of interaction force and the influence of other pedestrians within the unreasonable range on i are reduced by the neighborhood. So it could optimates the calculation performance.

2) Pedestrian View Angle

In the original SFM, pedestrians have a wild view angle. They can observe the position and motion state of things around them at any moment, which is not consistent with the experience. In reality, pedestrians observe in the direction they are going, and only in certain circumstances can they expand their view angle by turning their heads. In most cases, the pedestrian's view angle is limited to a reasonable range of deflection based on the direction of travel. Therefore, other pedestrians and obstacles within the i view angle at time t form an effective neighborhood pedestrian set ENP_i^t and an effective neighborhood obstacle set ENO_i^t, respectively. In this paper, the view angle of the SFM is improved in terms of person-to-person and person-to-obstacle situations:

a) Pedestrian to Pedestrian

$$ENP_i^t = \left\{ j \left| \ \varphi_{ij}^t < 90°, \forall i \in P, j \in NP_i^t, t \in T \right. \right\} \tag{11}$$

$$\vec{n}_{ji}^t = \frac{\vec{r}_i^t - \vec{r}_j^t}{\left\| \vec{r}_i^t - \vec{r}_j^t \right\|} \tag{12}$$

$$\varphi_{ij}^t = \arccos \frac{\vec{v}_i^t \cdot \vec{n}_{ji}^t}{\left\| \vec{v}_i^t \right\| \left\| \vec{n}_{ji}^t \right\|} \tag{13}$$

where $\vec{n}_{ji}^t$ denotes the unit vector of i pointing to j, $\vec{v}_i^t$ denotes the speed of i at time t, and φ_{ij}^t denotes the angle between the walking direction of i and the line between i and j. If $\varphi_{ij}^t < 90°$ and $j \in NP_i^t$, it means that j is in the

978-1-6654-9713-8/21/$31.00 ©2021 IEEE

view angle of i, and j joins the effective pedestrian set ENP_i^t of i at the moment t.

Eq.(11) can calculate the effective neighborhood pedestrian set. This set will be used as a variable set to calculate the mutual repulsive forces between different pedestrians. Therefore, the improved formula is shown as Eq. (14).

$$\vec{F}_i^{(p,t)*} = \sum_{j(i\neq j)} f_{ij}^t, j \in ENP_i^t \tag{14}$$

b) Pedestrian to Obstacle

Pedestrians have different sensitivities to obstacles and other pedestrians. Pedestrians at the same distance are more likely to approach obstacles than nearby pedestrians. In this paper, different view angle ranges are set to describe this phenomenon, as shown in Fig.2.

$$ENO_i^t = \left\{ o \middle| \ \varphi_{io}^t < 30°; i \in P, o \in NO_i^t \right\} \tag{15}$$

$$\vec{n}_{oi}^t = \frac{\vec{r}_i^t - \vec{r}_o^t}{\left\| \vec{r}_i^t - \vec{r}_o^t \right\|} \tag{16}$$

$$\varphi_{io}^t = \arccos \frac{\vec{v}_i^t \cdot \vec{n}_{oi}^t}{\left\| \vec{v}_i^t \right\| \left\| \vec{n}_{oi}^t \right\|} \tag{17}$$

By calculating Eq.(15), we can get the effective neighborhood obstacle set of i at time t. This set will be used as a set of variables to calculate the repulsive forces between pedestrians and obstacles. So, the improved formula as Eq.(18):

$$\vec{F}_i^{(o,t)*} = \left\{ f_{io}^t \middle| o = \min\left(d_{io}^t\right), o \in ENO_i^t \right\} \tag{18}$$

To sum up, the Improved SFM (ISFM) is shown as Eq. (19) :

$$\vec{F}_i^t = \vec{F}_i^{(d,t)} + \vec{F}_i^{(p,t)*} + \vec{F}_i^{(o,t)*} \tag{19}$$

$$\vec{a}_i^t = \frac{1}{m_i}\left(\vec{F}_i^{(d,t)} + \vec{F}_i^{(p,t)*} + \vec{F}_i^{(o,t)*} \right) \tag{20}$$

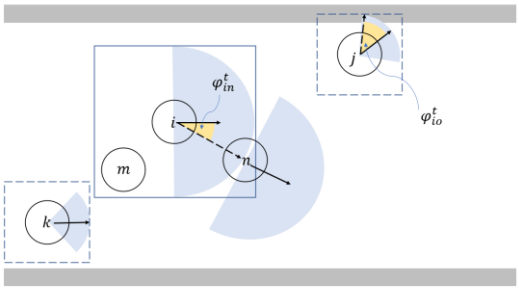

Fig. 2. Pedestrian view angle

III. ALGORITHM

A. The Simulation Method

In this paper, the simulation method is used to verify and analyze the model. We coded the ISFM with C#, and the simulation algorithm was designed with time-driven. The SFM calculates the acceleration of pedestrians by calculating the force acting on them at a certain moment. Within the time step $\Delta\tau$, the velocity of the pedestrian at time $t+\Delta\tau$ is updated by the acceleration $\vec{a}_i^t$. If the time step $\Delta\tau$ is too large, it will lead to the loss of simulation details or even the occurrence of pedestrian collisions, pedestrians over obstacles, and other unreasonable circumstances. Therefore, the simulation performance would be more practical with the smaller time step. However, the smaller the simulation step size, the more computer burden needs to carry out the calculation in the same simulation time, and the lower the efficiency of the calculation operation. Then, after many tests, $\Delta\tau = 0.01$s can achieve the trade-off between performance and efficiency.

B. The Simulation Algorithm

For the i, we assume that its relevant parameters are shown in Table I below:

TABLE I. PEDESTRIAN PARAMETERS TABLE

Parameter	Symbol	Reference Value
Adaptation time	τ_i	0.5s
Bodyweight	m_i	[45kg,85kg]
Radius	r_i	[0.19m,0.25m]
Expected speed	v_i^e	[1.1m/s,1.6m/s]
The intensity of the interaction between other pedestrians	A_i	$2\times10^3 N$
The influence distance of repulsive force between other pedestrians	B_i	0.08m
The intensity of the interaction between pedestrians and obstacles	A_i	$2\times10^3 N$
The influence distance of the repulsive force between pedestrians and obstacles	B_i	0.08m
Human body elasticity coefficient	K	$1.2\times10^5 N/m$
Human body sliding friction elasticity coefficient	k	$2.4\times10^5 N/m$

According to the set parameters, this paper designs Algorithm 1 to update the neighborhood sets of pedestrians, and Algorithm 2 to update the location of pedestrians.

Algorithm 1 Calculate the effective neighborhood pedestrian set and the effective neighborhood obstacle set

Input: P, O, t

1: **For** i **in** P, o **in** O
2: **For** j **in** P **and** $j \neq i$
3: **Compute** NP^t, NO^t by Eq.(9)(10)
4: **If** $NP^t \neq \varnothing$
5: **Compute** φ_{ij}^t by Eq.(13)
6: **Do** Eq.(11)
7: **If** $NO^t \neq \varnothing$
8: **Compute** φ_{io}^t by Eq.(17)
9: **Do** Eq.(15)
10: **End For**
11: **End For**

Output: ENP_i^t, ENO_i^t

Algorithm 2 Calculate the positions of all pedestrians over time (SFM)

Input: Initialize the obstacle position and pedestrian's bodyweight, radius, expected speed, initial position. The total simulation time is T, and the simulation time step is $\Delta\tau$

978-1-6654-9713-8/21/$31.00 ©2021 IEEE

1: **For** $t \leftarrow 0:T$ **do**
2: **For** I in P **do**
3: **Algorithm 2**
4: **If** $ENP_i^t \neq \varnothing$
5: **Compute** $\vec{F}_i^{(p,t)*}$ by Eq.(14)
6: **If** $ENO_i^t \neq \varnothing$
7: **Compute** $\vec{F}_i^{(o,t)*}$ by Eq.(18)
8: **Compute** $\vec{F}_i^{(d,t)}$ by Eq.(2)
9: **Compute** $\vec{F}_i^t$, $\vec{a}_i^t$, $\vec{v}_i^{t+\Delta\tau}$, $\vec{y}_i^{t+\Delta\tau}$ by Eq.(19)(20)(7)(8)
10: **End For**
11: $t = t + \Delta\tau$
12: **End For**
Output: $\vec{y}_i^t, \forall i \in P, t \in T$

IV. Numerical Experiments

In this section, several typical pedestrian flow scenes are simulated by the proposed ISFM to demonstrate its performance and efficiency.

A. Model Validation and Scenario Testing

1) A single-channel and one-way pedestrian flow

The channel width is set as 3m, the length is 15m, and the initial number of people is 180. Four moments t =0, 5, 10, 15 are selected in Fig.3(a)-(d) to show the movement process of pedestrians with time. It can be observed that the ISFM avoids the overlapping phenomenon, and pedestrians have the characteristics of avoiding, waiting, and following.

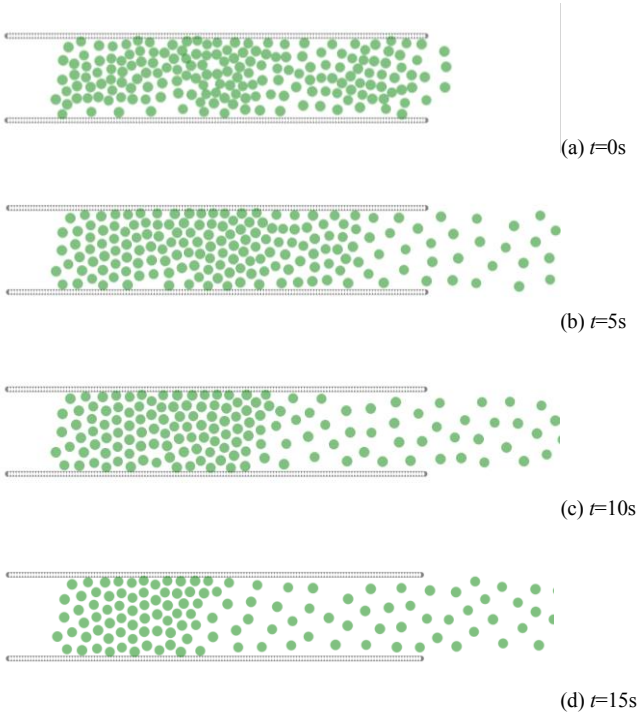

(a) t=0s (b) t=5s (c) t=10s (d) t=15s

Fig. 3. Single-channel and one-way pedestrian flow

For the scene of one-way pedestrian flow in the single channel, the relationship between density and speed is output in the simulation process, as shown in Fig.4.

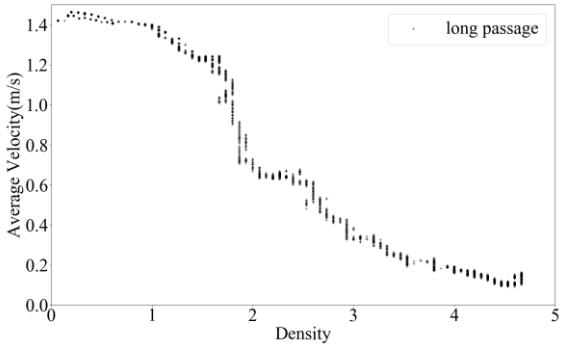

Fig. 4. Scatter diagram of density and velocity

It can be seen that with the increase of pedestrian density, the speed of pedestrians in the area presents a nonlinear decreasing trend. When the pedestrian density is within the range of [0, 1] per/m^2, the average pedestrian speed decreases relatively gently. When the pedestrian density changes between [1.5, 2.5] per/m^2, the average pedestrian speed decreases rapidly. When the pedestrian density is greater than 5 per/m^2, the average pedestrian speed tends to 0. This phenomenon is consistent with the pedestrian flow characteristic summarized from reality pedestrian flow experiments by the research of M.Mori and H. Thukaguchi.

2) Single Exit and one-way pedestrian flow

The Exit width is 1.3m, the initial number of pedestrians is set as 100. Four moments t =0, 5, 10, 25 are selected in Fig.5(a)-(d) to show pedestrians' movement and change process with time. As can be seen, due to the limitation of the exit capacity, pedestrians in this scene will gather at the Exit and present an arched waiting shape, which conforms to the empirical rule that a large number of pedestrians pass from a single exit.

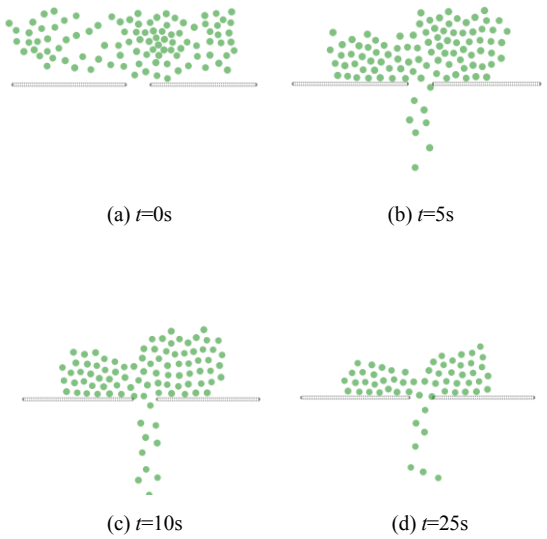

(a) t=0s (b) t=5s (c) t=10s (d) t=25s

Fig. 5. Single Exit and one-way pedestrian flow

In this paper, the number of one-way pedestrian flow at a single exit is set as 100, 80, 40, and 20, respectively, and the simulation durations are 20 seconds. In addition, the relationship between time and average pedestrian speed in the

978-1-6654-9713-8/21/$31.00 ©2021 IEEE

Exit area (as shown in Fig.6) is calculated, and the result is shown in Fig. 7.

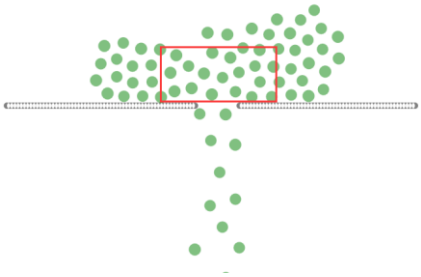

Fig. 6. The study area

According to Fig.7, when time interval is constant, the more people pass through the exit, the lower the average passing speed of the exit. The details are shown in Table II.

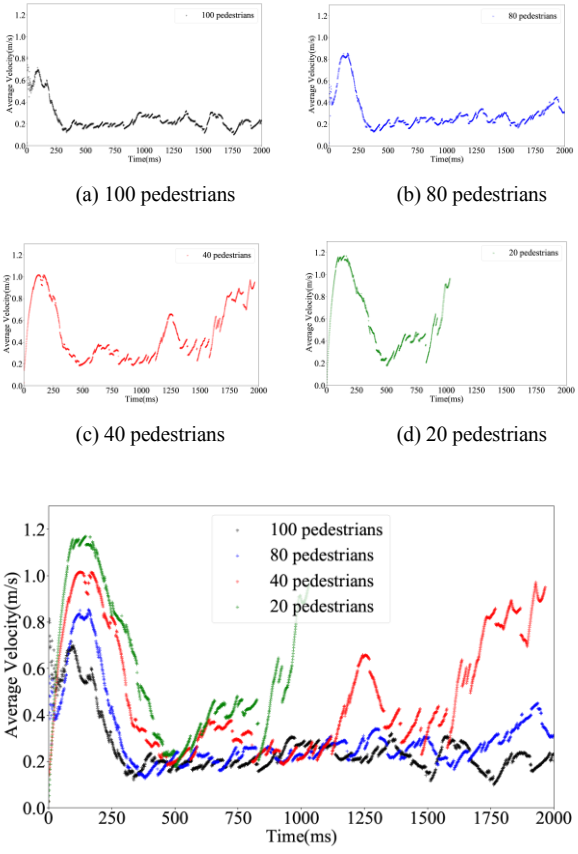

(a) 100 pedestrians (b) 80 pedestrians

(c) 40 pedestrians (d) 20 pedestrians

(e)

Fig. 7. The average pedestrian speed at different times with a different number of pedestrians in twenty seconds

TABLE II. DENSITY AND AVERAGE VELOCITY RELATION TABLE FOR DIFFERENT PEDESTRIAN NUMBER

Pedestrians' Number	**100**	**80**	**40**	**20**
Density(person/m^2)	2.946	2.620	1.332	0.495
Velocity(m/s)	0.253	0.299	0.478	0.589

At the same time, by observing the relationship between the time and the speed in the scatter diagram, we notice that when the number of pedestrians is 100, the speed at the bottleneck fluctuates with time (stop-and-go waves), as shown in Fig. 7(a). The speed fluctuates between 0.1m/s and 0.4m/s during [2, 20]s. As shown in Fig. 7(b), the velocity fluctuates between 0.1m/s and 0.4m/s during time [2.5, 19]s. When the number of people is low, the speed fluctuates for a short time; otherwise, the speed fluctuates for a long time, which is related to exit ability.

By resetting different pedestrians for simulation, we found that the speed difference generally existed at exit and long passage with high-density pedestrian flow. In reality, people moving in a queue will show the speed spread, and this phenomenon also exists in road traffic. It takes reaction time for people to judge whether moving forward from a standstill. The reaction time is different for each pedestrian. When the number of people is within a certain range, reaction time accumulation causing fluctuations in the average speed. It indicates that the ISFM can capture the phenomenon of pedestrian crowding propagation.

B. The Study of Metro Passenger Behavior

This chapter first defines the environment parameters to studying passengers' alighting and boarding behavior in the Metro. Metro trains are generally organized with six carriages in reality, and there are five doors on each side of each carriage for passengers alighting and boarding. The area in front of the train is divided into two parts. The first part is the alighting area, and the second part is two separate waiting areas, as shown in Fig.8. In this paper, a platform screen door is selected to study passengers' alighting and boarding behavior.

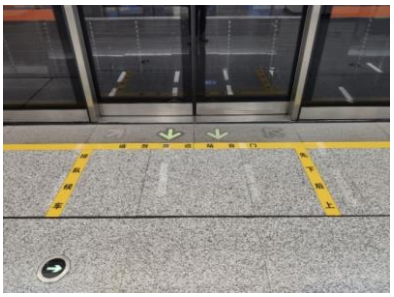

Fig. 8. Metro alighting and boarding area

In this paper, the simulation environment is set according to the practical data of Xingye North Street Metro Station in Chengdu. The width of the platform screen door is 2m, and the width of the train door is 1.5m. The boarding strategy of passengers is first alighting and then boarding. To study the relationship between the number and time of passengers alighting and boarding the carriage, we set a different number of people (varies from 2 to 40) based on ISFM to carry out the simulation. For example, while the number of people alighting and boarding the carriage are both 20, the changes in the position distribution of pedestrians at the four moments t =0,5,10,15 are shown in Fig.9(a)-(d)(Black dots denotes the alighting pedestrians, while gray dots denotes the boarding pedestrians).

978-1-6654-9713-8/21/$31.00 ©2021 IEEE

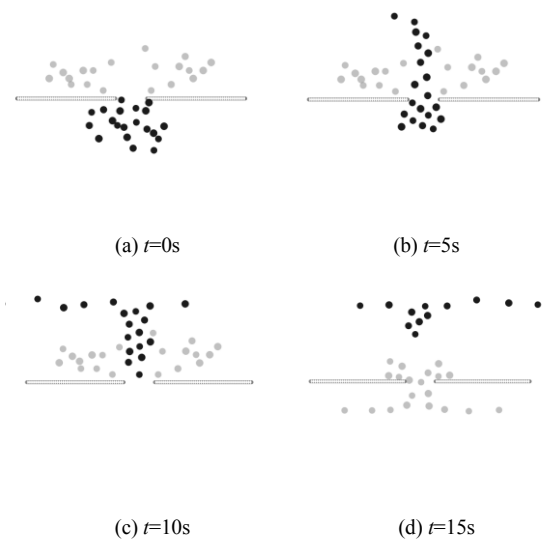

(a) t=0s (b) t=5s

(c) t=10s (d) t=15s

Fig. 9. Metro platform screen door pedestrian flow

As shown in Fig.10, the simulation experiment results show that with the number of passengers alighting and boarding the train increasing, the spent meantime will be longer. As the number of passengers increases, the more route conflicts between different passengers, the more potential pedestrian route conflicts. The average velocity of passengers will decrease with the rise of streamline intersection intensity. As shown in Fig.11 (a), the original SFM is used in this paper to calculate the time required alighting and boarding a metro platform screen door with a different number of passengers. The results show that the Pearson correlation coefficient of SFM and ISFM reaches 0.907, so the ISFM can reproduce the simulation effect of the original SFM. The average speed of pedestrians in the ISFM is lower than that of the original SFM because the view angle of pedestrians is added in the improved model, and people in normal walking will not be affected by the people behind them.

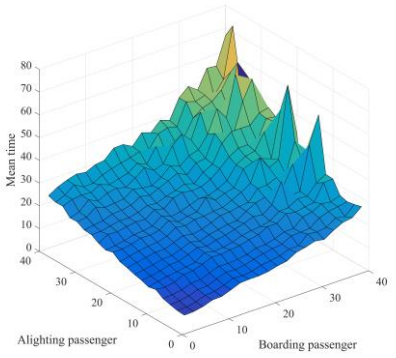

Fig. 10. Passenger alighting and boarding time

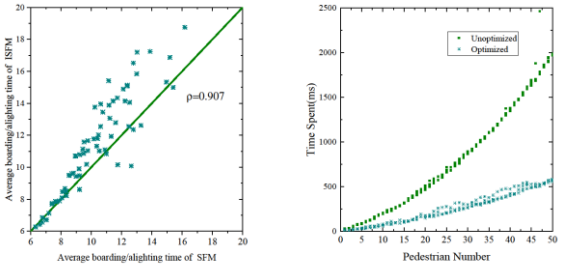

(a) (b)

Fig. 11. Passenger alighting and boarding time and algorithm efficiency

In addition, we also test the efficiency and stability of the algorithm. For the scene of alighting and boarding the train, we used the original algorithm and the optimization algorithm (which adding the neighborhood concept) to test the algorithm's efficiency (the number of simulated people varies from 1 to 50, and each simulation was conducted ten times). The results are shown in Fig.11 (b). The complexity of the unoptimized algorithm is $O(n^2)$, while the optimized algorithm is $O(n)$ and is n times quicker than unoptimized algorithm. Eq.(21) and (22) are the results of fitting the efficiency of the two algorithms.

$$y = 0.5139x^2 + 13.246x + 10.771 \tag{21}$$

$$y = 10.333x \tag{22}$$

V. CONCLUSION

Microscopic pedestrian simulation plays a vital role in traffic configuration design and traffic safety. In this paper, SFM is improved by adding pedestrian neighborhood and view angle sensitives and optimizing the algorithm. The ISFM maintains the accuracy of the original model and improves the simulation efficiency.

Our future research will further improve the SFM and add more scene judgments to realize pedestrians' active avoidance of obstacles and reasonable planning of walking paths, especially the avoidance of pedestrian flow conflicts.

ACKNOWLEDGEMENT

This research is supported by the National Natural Science Foundation of China (No. 71901183) and the Applied Basic Research Programs of Science and Technology Department of Sichuan Province (JDSKCXZX202001).

REFERENCES

[1] J. Fruin, “Designing for pedestrians: A level-of-service concept,” *Highw. Res. Rec.*, vol. 355, Jan. 1971.

[2] W. Daamen and S. P. Hoogendoorn, “Research on pedestrian traffic flows in the Netherlands,” *Proc. Walk 21 IV*, pp. 101–117, 2003.

[3] S. K. So and C. F. Daganzo, “Managing evacuation routes,” *Transp. Res. Part B Methodol.*, vol. 44, no. 4, pp. 514–520, May 2010, doi: 10.1016/j.trb.2009.11.002.

[4] M. Muramatsu, T. Irie, and T. Nagatani, “Jamming transition in pedestrian counter flow,” *Phys. Stat. Mech. Its Appl.*, vol. 267, no. 3, pp. 487–498, May 1999, doi: 10.1016/S0378-4371(99)00018-7.

[5] S. Okazaki and S. Matsushita, “A Study of Simulation Model for Pedestrian Movement with Evacuation and Queuing,” *Eng. Crowd Saf.*, vol. 432, Jan. 1993, doi: 10.3130/aijax.432.0_79.

[6] D. Helbing and P. Molnar, “Social Force Model for Pedestrian Dynamics,” *Phys. Rev. E*, vol. 51, no. 5, pp. 4282–4286, May 1995, doi: 10.1103/PhysRevE.51.4282.

[7] D. Helbing, I. Farkas, and T. Vicsek, “Simulating dynamical features of escape panic,” *Nature*, vol. 407, no. 6803, pp. 487–490, Sep. 2000, doi: 10.1038/35035023.

[8] S. Seer, C. Rudloff, T. Matyus, and N. Braendle, “Validating social force based models with comprehensive real world motion data,” in *Conference on Pedestrian and Evacuation Dynamics 2014 (ped 2014)*, vol. 2, W. Daamen, D. C. Duives, and S. P. Hoogendoom, Eds. Amsterdam: Elsevier Science Bv, 2014, pp. 724–732. doi: 10.1016/j.trpro.2014.09.080.

[9] Z. Kang, L. Zhang, and K. Li, “An improved social force model for pedestrian dynamics in shipwrecks,” *Appl. Math. Comput.*, vol. 348, pp. 355–362, May 2019, doi: 10.1016/j.amc.2018.12.001.

978-1-6654-9713-8/21/$31.00 ©2021 IEEE

[10] J. Wan, J. Sui, and H. Yu, "Research on evacuation in the metro station in China based on the Combined Social Force Model," *Phys. Stat. Mech. Its Appl.*, vol. 394, pp. 33–46, Jan. 2014, doi: 10.1016/j.physa.2013.09.060.
[11] X. Yang, X. Yang, F. Pan, Y. Kang, and J. Zhang, "The effect of passenger attributes on alighting and boarding efficiency based on social force model," *Phys. Stat. Mech. Its Appl.*, vol. 565, p. 125566, Mar. 2021, doi: 10.1016/j.physa.2020.125566.
[12] D. Helbing, L. Buzna, A. Johansson, and T. Werner, "Self-organized pedestrian crowd dynamics: Experiments, simulations, and design solutions," *Transp. Sci.*, vol. 39, no. 1, pp. 1–24, Feb. 2005, doi: 10.1287/trsc.1040.0108.
[13] Y. Sun and H. Liu, "Crowd evacuation simulation method combining the density field and social force model," *Phys. Stat. Mech. Its Appl.*, vol. 566, p. 125652, Mar. 2021, doi: 10.1016/j.physa.2020.125652.
[14] R. Mazzon and A. Cavallaro, "Multi-camera tracking using a Multi-Goal Social Force Model," *Neurocomputing*, vol. 100, pp. 41–50, Jan. 2013, doi: 10.1016/j.neucom.2011.09.038.
[15] X. Song, J. Sun, H. Xie, Q. Li, Z. Wang, and D. Han, "Characteristic time based social force model improvement and exit assignment strategy for pedestrian evacuation," *Phys. -Stat. Mech. Its Appl.*, vol. 505, pp. 530–548, Sep. 2018, doi: 10.1016/j.physa.2018.03.085.
[16] Y. Jiang, B. Chen, X. Li, and Z. Ding, "Dynamic navigation field in the social force model for pedestrian evacuation," *Appl. Math. Model.*, vol. 80, pp. 815–826, Apr. 2020, doi: 10.1016/j.apm.2019.10.016.
[17] I. M. Sticco, G. A. Frank, F. E. Cornes, and C. O. Dorso, "A re-examination of the role of friction in the original Social Force Model," *Saf. Sci.*, vol. 121, pp. 42–53, Jan. 2020, doi: 10.1016/j.ssci.2019.08.041.

978-1-6654-9713-8/21/$31.00 ©2021 IEEE